Journal of Materials Chemistry A

ROYAL SOCIETY OF CHEMISTRY

PAPER

View Article Online
View Journal | View Issue

Cite this: J. Mater. Chem. A, 2023, 11, 20592

First-principles study of intrinsic and hydrogen point defects in the earth-abundant photovoltaic absorber Zn_3P_2†

Zhenkun Yuan, Yihuang Xiong and Geoffroy Hautier *

Published on 10 september 2023. Downloaded on 17.10.2024 19:53:00.

Received 23rd June 2023
Accepted 9th September 2023

DOI: 10.1039/d3ta03697a

rsc.li/materials-a

Zinc phosphide (Zn_3P_2) has had a long history of scientific interest largely because of its potential for earth-abundant photovoltaics. To realize high-efficiency Zn_3P_2 solar cells, it is critical to understand and control point defects in this material. Using hybrid functional calculations, we assess the energetics and electronic behavior of intrinsic point defects and hydrogen impurities in Zn_3P_2. All intrinsic defects are found to act as compensating centers in p-type Zn_3P_2 and have deep levels in the band gap, except for zinc vacancies which are shallow acceptors and can act as a source of doping. Our work highlights that zinc vacancies rather than phosphorus interstitials are likely to be the main source of p-type doping in as-grown Zn_3P_2. We also show that Zn-poor and P-rich growth conditions, which are usually used for enhancing p-type conductivity of Zn_3P_2, will facilitate the formation of certain deep-level defects (P_{Zn} and P_i) which might be detrimental to solar cell efficiency. For hydrogen impurities, which are frequently present in the growth environment of Zn_3P_2, we study interstitial hydrogen and hydrogen complexes with vacancies. The results suggest small but beneficial effects of hydrogen on the electrical properties of Zn_3P_2.

1. Introduction

The II–V semiconductor zinc phosphide (Zn_3P_2) is a promising light-absorbing material for cost-effective thin-film photovoltaics.[1,2] It consists of earth-abundant elements and shows attractive optoelectronic properties as a solar absorber: a direct band gap of ~1.5 eV, a high absorption coefficient of over 10^4 cm^{-1},[3,4] and minority-carrier diffusion lengths (in the bulk crystal) of up to a few micrometers.[5,6] Zn_3P_2-based solar cells received considerable attention from the late 1970s to the 1990s. However, the efficiencies have been achieved as yet are far below the Shockley–Queisser limit (~33%).[7–12] The highest efficiency of Zn_3P_2 solar cells was reported in 1981 and has remained since then at just 5.96%.[8]

More recently, Zn_3P_2 solar cells have seen a resurgence of interest. Notably, researchers have developed fabrication methods for highly crystalline, reproducible Zn_3P_2 thin films on commercially available substrates which had long been a challenge.[13–15] The attainment of high-quality samples paves the way for addressing another persistent challenge: control of point defects and doping in bulk Zn_3P_2.[16,17]

As-grown Zn_3P_2 crystals and thin films nearly always exhibit p-type conductivity, the origin of which is believed due to intrinsic point defects.[18] Because conductivity has been observed to vary with the phosphorus partial pressure in the growth or annealing environment, it has been commonly attributed to phosphorus interstitials (P_i).[12,18–21] Despite no direct experimental observations of phosphorus interstitials or their involvement in p-type doping, this assignment has been supported by an early first-principles investigation based on semilocal density-functional theory (DFT), which has suggested that phosphorus interstitials are the most prevalent acceptor species in Zn_3P_2.[22] However, a subsequent first-principles study, using more accurate hybrid functional, has shown that P_i is a deep acceptor and has much higher formation energy than another acceptor, the zinc vacancy (V_{Zn}).[23] In order to clarify these conflicting results, recently Stutz *et al.* and Paul *et al.* studied the effect of compositional stoichiometry variations on the structural, electrical, and optical properties of monocrystalline Zn_3P_2 thin films, yet a conclusive identification of the source for the p-type conductivity, whether it is due to P_i or V_{Zn}, has remained elusive.[24,25] On the other hand, less attention has been devoted to identifying deep-level defects in Zn_3P_2, in spite of accumulating experimental evidence for presence of deep levels in the band gap of Zn_3P_2.[26–28] Deep-level defects may act as nonradiative carrier recombination centers which would limit the efficiency of Zn_3P_2 solar cells.

In addition to intrinsic defects, there is strong experimental evidence that hydrogen impurities are likely present in Zn_3P_2 samples: growth of Zn_3P_2 thin films is conventionally carried out in H_2 atmosphere and/or PH_3 gas using techniques such as physical vapor transport,[4,29] chemical vapor deposition[30,31] and metal–organic chemical vapor deposition,[32–35] ionized cluster

Thayer School of Engineering, Dartmouth College, Hanover, New Hampshire 03755, USA. E-mail: geoffroy.hautier@dartmouth.edu

† Electronic supplementary information (ESI) available. See DOI: https://doi.org/10.1039/d3ta03697a

This journal is © The Royal Society of Chemistry 2023

Published on 10 september 2023. Downloaded on 17.10.2024 19:53:00.

beam deposition,[36] and RF sputtering.[37,38] Sometimes the samples were also annealed in H_2 gas following growth.[33,37,39–41] It is known that unintentional hydrogen doping in oxides and III–V nitrides has a strong impact on the electrical properties of these materials.[42–44] Therefore, in order to avoid uncontrolled influence of hydrogen impurities, it is important to understand the behavior of hydrogen in Zn_3P_2.

Using first-principles calculations with a hybrid functional, we study intrinsic point defects and hydrogen impurities in Zn_3P_2: zinc and phosphorus vacancies (V_{Zn} and V_P), interstitials (Zn_i and P_i), and antisites (Zn_P and P_{Zn}); for hydrogen impurities, hydrogen interstitial (H_i) and hydrogen-vacancy complexes are investigated. The present work assesses the energetics and electronic behavior of the defects based on their calculated formation energies and charge transition levels. Comparing our results with experiments and previous calculations, we address the open questions about the shallow or deep nature of the defects in Zn_3P_2. Our work clarifies the likely defects leading to p-type doping in Zn_3P_2 and the possible deep-level defects which may act as nonradiative recombination centers. It also elucidates the role of hydrogen in doping of Zn_3P_2.

2. Intrinsic point defects

We have performed hybrid functional calculations for the intrinsic defects V_{Zn}, V_P, Zn_i, P_i, Zn_P, and P_{Zn} in Zn_3P_2. Fig. 1 shows the calculated formation energies for these defects, under Zn-poor (P-rich) and Zn-rich (P-poor) chemical-potential conditions. Details about the calculation methods and the chemical potentials of Zn and P can be found in the Methods section. We find, in Fig. S1 of the ESI,† a rather small chemical-potential region for which Zn_3P_2 is thermodynamically stable, due to strong phase competition from ZnP_2 (another stable crystalline phase in the Zn–P system).[45] Note that the terms "rich" and "poor" used in Fig. 1 and S1† do not represent the actual compositional stoichiometry of experimental samples but rather they correspond to the endpoints of the chemical-potential region that stabilizes compositionally stoichiometric Zn_3P_2, so the results presented in Fig. 1 are for the intrinsic defects in (nearly) stoichiometric samples.

As shown in Fig. 1, the V_{Zn} and Zn_i behave exclusively as an acceptor and as a donor, respectively. In contrast, all other intrinsic defects, including V_P, P_i, Zn_P, and P_{Zn}, are amphoteric: they exist in donor states when the Fermi level is low in the band gap while in acceptor states when the Fermi level is high in the band gap. The amphoteric behavior of these defects is related to the unique ability for phosphorus to occur in multiple oxidation states from P^{3-} to P^{5+}.

We find that the V_{Zn} behaves as a shallow acceptor and is the only intrinsic defect that can act as a source of p-type doping in Zn_3P_2. The V_{Zn} gives rise to two acceptor levels in the band gap: a shallow (0/−) transition level at 0.11 eV and a relatively deep (−/2−) transition level at 0.23 eV above the valence band (see Fig. 1). For reference, the calculated single-particle defect states of V_{Zn} can be found in Fig. S2 of the ESI.† The formation energy of V_{Zn} is relatively high for Fermi-level positions close to the valence-band maximum (VBM), even under Zn-poor/P-rich condition.

Contrary to the commonly accepted assumption that phosphorus interstitials are the cause of p-type conductivity in as-grown Zn_3P_2,[12,18–21] we find that phosphorus interstitials cannot possibly contribute to p-type doping. First and foremost, P_i gives rise to a very deep acceptor level $\varepsilon(0/-) = 0.69$ eV (see Fig. 1); thus, it can hardly provide holes to the valence band through thermal excitation. Second, for most Fermi-level

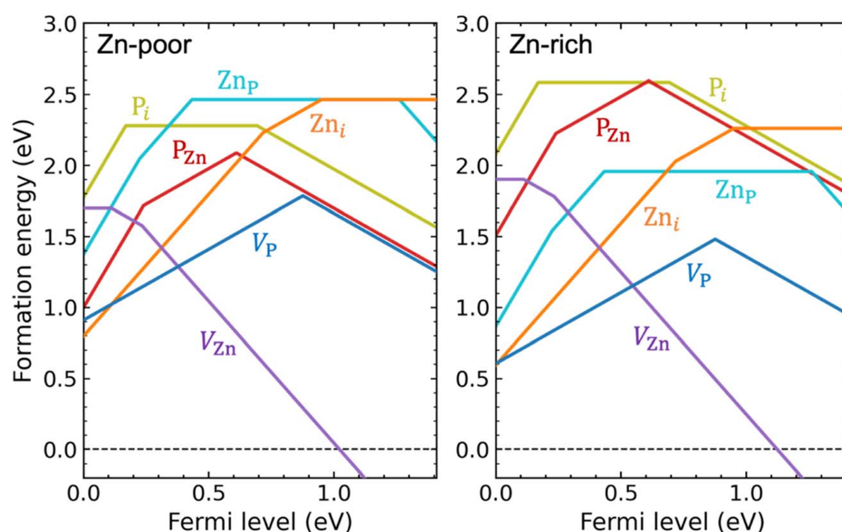

Fig. 1 Formation energies as a function of Fermi level for intrinsic point defects in Zn_3P_2, under Zn-poor/P-rich (left) and Zn-rich/P-poor (right) conditions. The zero of the Fermi level is set at the VBM and the upper bound corresponds to the conduction-band minimum (CBM). For the same Fermi-level value, only formation energy for the most stable charge state is shown, *i.e.*, V_{Zn}: 0, −, 2−; V_P: +, −; Zn_i: 2+, +, 0; P_i: 3+, 0, −; Zn_P: 3+, 2+, 0, 2−; P_{Zn}: 3+, +, −. Kinks in each curve indicate transitions between different charge states (values of the thermodynamic transition levels are also listed in Table S1 of the ESI†).

Published on 10 september 2023. Downloaded on 17.10.2024 19:53:00.

positions in the lower part of the band gap, P_i will exist in the neutral charge state (being electrically inactive). Even when the Fermi level is close to the valence band, P_i can also be stable in the +3 charge state, with a (3+/0) transition level at 0.17 eV above the VBM. The existence of this positive charge state, which removes three holes from the valence band, suggests that phosphorus interstitials could act as compensating centers in p-type Zn_3P_2 (though this happens for Fermi level below 0.17 eV). Third, P_i has a high formation energy and is therefore not expected to form in significant concentrations in (nearly) stoichiometric Zn_3P_2 samples.

Fig. 2a shows that in the neutral charge state, the P_i adopts a split-interstitial configuration in which the interstitial P shares a lattice site with one of the lattice P atoms, consistent with previous calculations.[22,23] Similar split-interstitial configuration has been found for the nitrogen interstitial in GaN.[46] The plotted spin density shows that the neutral P_i is characterized by a highly localized hole state, with most of the charge located on the interstitial P atom and the bonded lattice P atom. The calculated single-particle energy level of the hole state is located well above the VBM (more specifically, right below the CBM), as indicated by the blue line in Fig. 2b. When the P_i becomes negatively charged, there is a large relaxation of the interstitial and the surrounding atoms, yet the split-interstitial configuration is largely kept, as shown in Fig. 2c. As a result, the single-particle defect level is pushed down to below the VBM, as indicated by the red line in Fig. 2b. Interestingly, as indicated by the black dashed line in Fig. 2b, the average of the two single-particle defect levels is 0.62 eV above the VBM, which happens to provide a good estimate of the (0/−) transition level (0.69 eV).

All other intrinsic defects, including V_P, Zn_i, Zn_P, and P_{Zn}, have deep transition levels in the band gap, as seen in Fig. 1. The Zn_i is a double donor with two deep levels: a (+/0) transition level at 0.95 eV and a (2+/+) transition level at 0.72 eV above the VBM. For V_P, the formation energies of V_P^+ and V_P^- intersect at 0.88 eV above the VBM, and V_P^0 is energetically unstable compared to either V_P^+ or V_P^- over the entire range of Fermi-level positions in the band gap; this is characteristic of a negative-U behavior. Similar to V_P, the P_{Zn} forms a deep transition level between +1 and −1 charge states at 0.61 eV above the VBM. The Zn_P has a deep (2+/0) transition level (also a negative-U transition) at 0.43 eV above the VBM. Besides these deep levels, the P_{Zn} (3+/+) transition level is close to the VBM, and the Zn_P (3+/2+) and (0/2−) transition levels are close to the VBM and CBM, respectively.

Similar to the P_i, the V_P, Zn_P, and P_{Zn} will contribute to compensation in p-type Zn_3P_2, due to their amphoteric behavior. As indicated in Fig. 1, the V_P and Zn_i are the main

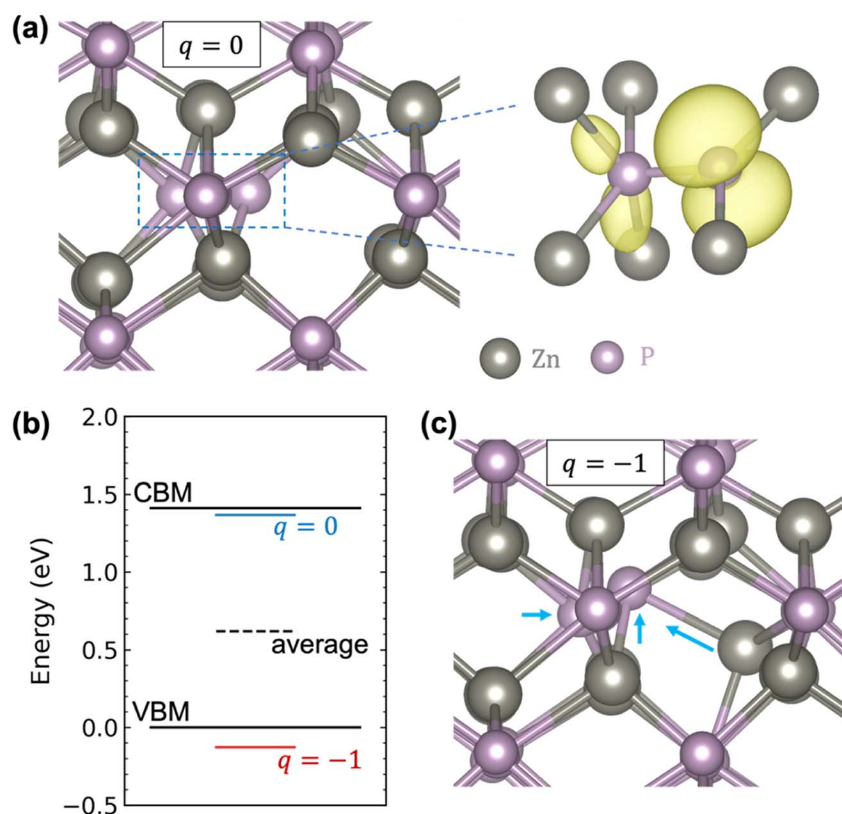

Fig. 2 (a) Local atomic geometry and spin density (isosurface at 10% of the maximum in yellow) associated with the localized hole state of the P_i in the neutral charge state ($q = 0$). The P_i adopts a split-interstitial configuration in which the interstitial P shares a lattice site with a lattice P atom. (b) Single-particle energy levels of the localized hole state of the P_i, before and after being occupied (with both atomic and electronic relaxations). The energy of the VBM is set to zero. To plot the single-particle defect levels and the bulk band edges (the VBM and CBM) together, a simple alignment using the deep core level of the farthest atom from the defect site is considered. (c) Local atomic geometry of the P_i in the $q = -1$ charge state, with the arrows indicating the local atomic relaxations.

 This journal is © The Royal Society of Chemistry 2023

Published on 10 september 2023. Downloaded on 17.10.2024 19:53:00.

compensating intrinsic defects in p-type Zn_3P_2. In addition, depending on growth conditions and on the p-type doping level (*i.e.*, the Fermi-level position), the formation energy of Zn_P and P_{Zn} can be as low as ~1 eV, suggesting that both defects can form in significant concentrations and thus also be important compensating centers. From Fig. 1 we can see that compensation of p-type doping is reduced under Zn-poor/P-rich condition where the V_P and Zn_i have higher formation energy (though the formation energy of P_{Zn} is lowered under this condition).

3. Comparison with experiments and discussion

The type of possible doping or dopability of a material are largely controlled by compensation. Hole-killer (electron-killer) defects can prevent p-type (n-type) doping.[47,48] Our first-principles results indicate that Zn_3P_2 clearly favors p-type doping, because no hole-killer defects will pin the Fermi level while the electron-killer V_{Zn} will pin the Fermi level and prevent n-type doping even in the presence of shallow extrinsic donors. The p-type doping of Zn_3P_2 is favored under Zn-poor/P-rich conditions, where both the formation energy of V_{Zn} acceptors and the compensation will be reduced. Our finding agrees with the experimentally observed p-type nature of Zn_3P_2.[12,18–21]

Our results suggest that V_{Zn} (but not P_i) is a source of p-type conductivity in as-grown Zn_3P_2. This disagrees with the previous reports that p-type conductivity in Zn_3P_2 is due to P_i which has been based on experimental observations that conductivity of Zn_3P_2 samples varies with the phosphorus partial pressure in the growth or annealing environment.[12,18–21] Here we take a closer look at ref. 18 and 19. In ref. 18, Zn_3P_2 samples were post-growth annealed over a range of equilibrium vapor compositions, and conductivity was observed to be increased when changing from Zn-rich annealing conditions (zinc vapor) to P-rich annealing conditions (phosphorus vapor). In ref. 19, electrical measurements were performed on a set of samples with the P/(Zn + P) ratio varying from 0.39 (which corresponds to a P-poor sample) to 0.4 (which corresponds to a stoichiometric sample), showing increased conductivity. For both studies, the observed conductivity increase can be explained by an enhancement of the V_{Zn} concentration and a reduction of the V_P and Zn_i concentrations. It should be noted that since Zn_3P_2 is a binary compound, a P-rich (P-poor) condition means a Zn-poor (Zn-rich) condition. We conclude that our results are in line with the experimental observations.

The more recent experimental work by Stutz *et al.*,[24] is also of interest. This work studied monocrystalline, nonstoichiometric P-rich Zn_3P_2 thin films and found increasing lattice expansion when the compositional stoichiometry varies from $Zn_{2.98}P_{2.02}$ (Zn/P = 1.47) to $Zn_{2.75}P_{2.25}$ (Zn/P = 1.22) to $Zn_{2.67}P_{2.33}$ (Zn/P = 1.15). Stutz *et al.* interpreted their results in terms of the formation of P_i, and also suggested that many of the defects in their samples are in neutral charge state (based on the fact that in all three samples, the compositionally induced defect density is about five orders of magnitude higher than carrier density). Our results support the analysis of Stutz *et al.*, whereas further indicate that it is necessary to account for the P_{Zn} in understanding the defects in non-stoichiometric P-rich Zn_3P_2 samples; that is, an excess of P leads to P_{Zn} and P_i and facilitates the formation of V_{Zn}. In this case, the V_{Zn} acceptors are expected to be heavily compensated by P_{Zn}, and most P_i defects will be in the neutral charge state as discussed above. Within this picture, non-stoichiometric P-rich Zn_3P_2 samples should be highly compensated.

Fig. 3 shows a comparison of our calculated positions of charge transition levels with experimental values obtained by deep-level transient spectroscopy (DLTS; on Zn_3P_2 polycrystals),[27,28] electrical transport measurements (on Zn_3P_2 single crystals),[26] and photoluminescence spectroscopy (on monocrystalline, nonstoichiometric P-rich Zn_3P_2 thin films).[24] Note that the experimental results have been classified as acceptor levels or hole-trap levels in the original work. In Fig. 3 we also plot the relevant transition levels involving thermodynamically unstable charge states: the (+/0) and (0/−) transition levels of both V_P and P_{Zn}, and the (2+/+) and (+/0) transition levels of Zn_P (for more information on the charge-state transitions we refer to Fig. S3 of the ESI†); such levels may be detected by transient spectroscopies like DLTS, but a more likely explanation is the presence of complex defects. In the following, we attempt to identify the origin of the experimentally observed defect levels. This assignment is tentative and based purely on the defect energy levels. It does not take into account defect clusters, extended defects, or extrinsic impurities which could be present in the experimental samples.[49]

First, we assign the acceptor level lying at ~0.14–0.2 eV, commonly observed in the experiments, to the (−/2−) transition level of V_{Zn}. In ref. 26 and another electrical transport experiment,[50] it has been found that in Zn_3P_2 samples with high hole density (~10^{17} cm^{-3}), there is only one important acceptor level lying at ~0.05 eV. This shallow acceptor level is assigned tentatively to the (0/−) transition level of V_{Zn}. Second, for the experimentally observed hole-trap levels, our speculations are as follows. The level lying at 0.25–0.30 eV (observed by electrical transport

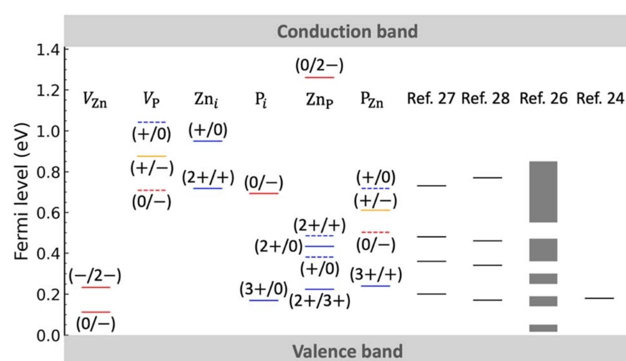

Fig. 3 Comparison of our calculated thermodynamic transition levels (between different charge states q and q') with experimental values reported in the literature. The red, blue, and orange solid lines indicate the calculated acceptor, donor, and (+/−) transition levels, respectively. The dashed lines indicate the relevant transition levels involving thermodynamically unstable charge states. Experimental data are taken from ref. 24 and 26–28; they have been reported as acceptor levels or hole-trap levels in the original work.

Published on 10 september 2023. Downloaded on 17.10.2024 19:53:00.

measurements) is assigned tentatively to the P_{Zn} (3+/+) transition level. The level lying at ~0.35 eV (detected by DLTS) is identified tentatively as the Zn_P (+/0) transition level. The level lying at ~0.46 eV (DLTS) may be assigned to Zn_P (2+/0) or (2+/+) or P_{Zn} (0/−) transition levels. The level lying at ~0.75 eV (DLTS) may be related to the V_P (0/−), Zn_i (2+/+), P_i (0/−), or P_{Zn} (+/0) transitions.

Deep levels in a solar absorber could cause nonradiative recombination of photo-generated carriers and hence be detrimental to the device performance.[51–54] Our identification of the intrinsic defects having deep levels in Zn_3P_2 will help optimize the absorber by control of these defects. However, suppressing the formation of the deep-level defects is likely to be challenging for Zn_3P_2. For instance, while Zn-poor/P-rich conditions are needed to enhance p-type doping, such conditions will facilitate the formation of P_{Zn} and P_i which possess deep levels. This implies that good photovoltaic performance is not guaranteed for nonstoichiometric P-rich Zn_3P_2 samples which have become the focus of recent experimental studies.[17,24,25] This analysis would however require a systematic study of the nonradiative carrier capture coefficients (cross sections) which could vary considerably between different deep levels,[55–59] which is beyond the scope of the present work.

4. Comparison with previous calculations

The first DFT study of intrinsic defects in Zn_3P_2 by Demers *et al.* used a semilocal functional.[22] One of the main conclusions of ref. 22 is that phosphorus interstitials are the most prevalent acceptors. Because of the inherent limitations of semilocal functionals in predicting band gaps for semiconductors,[60–62] Demers *et al.* corrected the band gap of Zn_3P_2 using an extrapolation method that is often difficult to justify.[60] In light of this deficiency, we believe that the calculated defect energetics in ref. 22 suffer from considerable uncertainties.

On the other hand, Yin *et al.* have reported hybrid-functional calculations for intrinsic defects in Zn_3P_2.[23] Both our results and those of Yin *et al.* agree that: (i) the V_{Zn} behaves as a shallow acceptor; (ii) the P_i gives rise to a deep acceptor level, and is energetically less favorable than V_{Zn}. However, some notable differences exist. As listed in Table S2 of the ESI,† the charge transition levels reported by Yin *et al.* are systematically shallower than ours. For instance, the (0/−) transition level of P_i is 0.30 eV in ref. 23 while it is 0.69 eV in the present work. In addition, Yin *et al.* have shown that V_P and P_i behave exclusively as a donor and as an acceptor, respectively, while we find amphoteric behavior of both defects. We attribute these discrepancies to the apparent lack of spin polarization and proper supercell-size corrections in the defect calculations in ref. 23.

5. Effects of hydrogen on doping and defect passivation

We now turn to hydrogen impurities in Zn_3P_2. We have considered hydrogen interstitial (H_i) and hydrogen in zinc and phosphorus vacancies, and performed a careful search for their lowest-energy configurations. It is seen in Fig. S4 of the ESI† that H_i^0 and H_i^- are most stable at the tetrahedral site and H_i^+ is most stable at the bond-center site. For a single H in the zinc vacancy, we initially incorporated it on the substitutional Zn site but found that it moves off to bind with one of the four surrounding P atoms; it is thus regarded as a H + V_{Zn} complex rather than a substitutional H_{Zn}. The V_{Zn} can trap a second H to form a 2H + V_{Zn} complex in which each H binds with one P atom. For a single H in the phosphorus vacancy, the H is also located off-center but binds with two Zn atoms, resulting in a H + V_P complex.

Fig. 4 plots the calculated formation energies for the H-related point defects, under Zn-poor/P-rich condition (as in Fig. 1) and at two different chemical potentials of H (μ_H): (i) $\mu_H = 0$, *i.e.*, the H-rich limit; (ii) a lower μ_H of −0.45 eV (this value is a more realistic choice of μ_H; it can be obtained through equilibrium with H_2 gas at 400 °C and partial pressure of 0.01 atm in the ideal-gas model;[63,64] see the Methods section). Let us first analyze the electronic behavior of the H-related defects. As can be seen, H_i is amphoteric with a (+/−) transition level in the band gap, as commonly found for hydrogen interstitial in semiconductors.[65] Since the (+/−) transition level is 0.57 eV above the VBM, H_i acts as a compensating center in p-type Zn_3P_2. Further, hydrogen passivates the dangling bonds of the vacancies and hence reduce their charge states. The H + V_{Zn} complex is a single acceptor with a (0/−) transition level 0.09 eV above the VBM, which is slightly shallower than that of isolated V_{Zn} (0.11 eV). The 2H + V_{Zn} complex has no gap states and does not introduce any defect level in the band gap. The H + VP complex is a single donor with a (+/0) transition level just 0.13 eV above the VBM.

Under the H-rich limit (left panel of Fig. 4), we see that the H_i^+, H + V_{Zn}, and 2H + V_{Zn} have low formation energy. In contrast, the H + V_P has relatively high formation energy. Here and in the following, our implicit assumption is that we are considering p-type Zn_3P_2. Moving to the lower μ_H (right panel of Fig. 4), the formation energies of the H-related defects are increased, especially for the 2H + V_{Zn} complex. In addition, the formation energy of H + V_{Zn} and 2H + V_{Zn} becomes comparable to that of isolated V_{Zn}. Irrespective of μ_H, the binding energy of $[H + V_{Zn}]^-$ (2H + V_{Zn}), defined as the difference between the formation energy of $[H + V_{Zn}]^-$ (2H + V_{Zn}) and the sum of the formation energies of isolated V_{Zn}^{2-} and H_i^+, is found to be 1.2 eV (2.0 eV). This is quite a large value, indicating that hydrogen interacts strongly with zinc vacancies resulting in stable complexes. The binding energy of the H + V_P with respect to isolated V_P^- and H_i^+ is also found to be large (1.43 eV). This suggests that the H + V_P complex would be stable if formed, despite having a relatively high formation energy. We also take note of the fact that interstitial hydrogen is expected to be quite mobile in crystalline semiconductors.[66–68]

It is thus found that when incorporated into Zn_3P_2, hydrogen is likely to form H_i^+ and stable complexes with the V_{Zn} acceptors. Because, compared with isolated V_{Zn}, the H + V_{Zn} has shallower acceptor level and lower formation energies (under H-rich conditions), hydrogen incorporation may enhance p-type doping of Zn_3P_2. As shown in Fig. S5 of the ESI,† the calculated bulk hole density increases as μ_H approaches zero (the H-

 This journal is © The Royal Society of Chemistry 2023

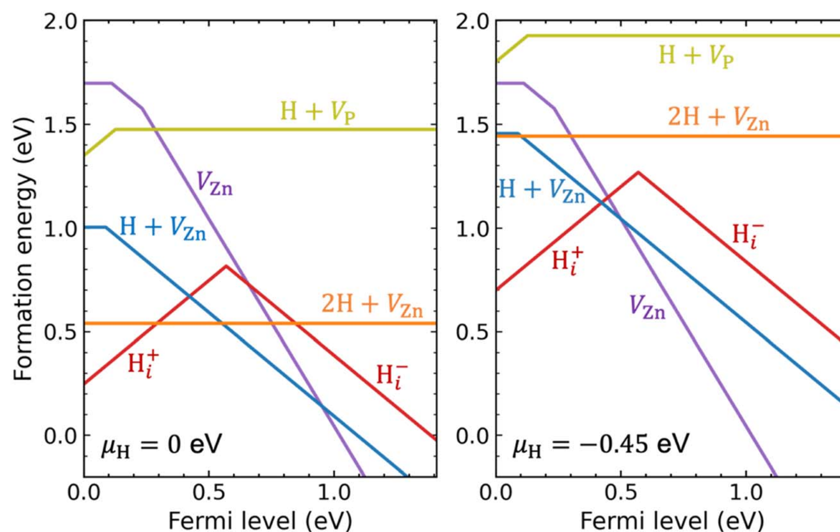

Fig. 4 Formation energies as a function of Fermi level for hydrogen interstitial (H_i) and hydrogen-vacancy complexes, including the $H + V_{Zn}$, $2H + V_{Zn}$, and $H + V_P$, in Zn_3P_2, under Zn-poor/P-rich condition and at two different chemical potentials of H (μ_H): the H-rich limit $\mu_H = 0$ eV (left panel) and a lower μ_H at −0.45 eV (right panel). For comparison the formation energy of V_{Zn} is also depicted.

Published on 10 september 2023. Downloaded on 17.10.2024 19:53:00.

rich limit). Nevertheless, the enhancement of p-type doping by $H + V_{Zn}$ is found to be small, because of the compensation by H_i^+ and the competition from $2H + V_{Zn}$ (which is electrically inactive).

We are aware of the experimental work of Wang *et al.*[39] and Bube,[40] which show increased bulk hole density (by about an order of magnitude) in Zn_3P_2 samples as a result of high-temperature annealing in H_2 gas. Yet, Bube[40] noted a depletion of holes in the surface region of the samples after the annealing. Suda *et al.*[37] reported that annealing Zn_3P_2 films in H_2 gas reduces the resistivity by an order of magnitude. In another study, Suda *et al.*[27] found that hydrogen plasma treatment of Zn_3P_2 removes a native hole-trap level at 0.2 eV above the VBM, which can be explained by passivation of V_{Zn}. Suda *et al.* also observed hydrogen passivation of deep hole-trap levels, and found that excessive hydrogenation creates a new hole-trap level at 0.13 eV above the VBM, which may be explained by formation of the H + VP complex. For hydrogen incorporation during the deposition of Zn_3P_2 films, Kakishita *et al.*[36] found only a passivation effect of hydrogen, but not change in conductivity.

6. Conclusions

In conclusion, we have studied intrinsic point defects and hydrogen impurities in Zn_3P_2 using first-principles hybrid functional calculations. Among the intrinsic defects, only zinc vacancies are shallow acceptors and can act as a source of p-type doping. All other intrinsic defects, including the V_P, Zn_i, P_i, Zn_P, and P_{Zn}, will contribute to compensation in p-type Zn_3P_2. All of these defects are amphoteric (except for the Zn_i which is exclusively a donor), and they all have deep levels in the band gap. Control of the intrinsic defects by adjusting the growth conditions to enhance p-type doping may be challenging for Zn_3P_2 if the concentration of the deep-level defects has to be kept low. For instance, while Zn-poor/P-rich growth or annealing conditions are needed to enhance the concentration of V_{Zn} acceptors, such conditions will facilitate the formation of the deep P_{Zn} and P_i defects. Hydrogen impurities in Zn_3P_2 are likely to form H_i^+ and stable complexes with the V_{Zn} acceptors. The $H + V_{Zn}$ complex is a shallow acceptor which can contribute to doping, while the H_i^+ will lead to compensation of holes and the $2H + V_{Zn}$ complex is electrically inactive. Due to the counteracting behavior of the H-related defects, the impact of hydrogen on p-type doping of Zn_3P_2 is predicted to be small.

7. Methods

All the DFT calculations were performed using the projector augmented wave (PAW) pseudopotential method and hybrid functional of Heyd–Scuseria–Ernzerhof (HSE) as implemented in the VASP code.[69–71] The wave functions were expanded in a plane-wave basis set with an energy cutoff of 400 eV. The tetragonal unit cell of Zn_3P_2 contains 40 atoms, and the Brillouin zone was sampled with a 4 × 4 × 3 Monkhorst–Pack *k*-point mesh. The HSE mixing parameter (α) was set to 0.32, which yields a band gap $E_g = 1.41$ eV and lattice parameters $a = 8.076$ Å and $c = 11.388$ Å for the unit cell, in agreement with the experimental values ($E_g \sim 1.5$ eV, and lattice parameters $a = 8.09$ Å and $c = 11.45$ Å).[4,72] This α value (0.32) was adopted in previous HSE hybrid-functional calculations in ref. 23; for consistency and comparison with ref. 23, we chose to use the same α value, instead of using a very slightly higher α to obtain a "perfect" match to the experimental band gap. A 2 × 2 × 2 supercell (which contains 320 atoms when it is defect free) was used for point-defect simulations, with a Γ-only *k*-point for the Brillouin-zone sampling. All atomic coordinates in supercells containing a point defect were fully relaxed until the residual atomic forces become less than 0.01 eV Å^{-1}. Spin polarization was explicitly considered in all the defect calculations. Defect

Published on 10 september 2023. Downloaded on 17.10.2024 19:53:00.

formation energies and thermodynamic charge transition levels were calculated using the standard first-principles formalism as detailed in ref. 61 and the PyCDT code.[73] For charged defects, electrostatic correction and potential alignment were applied using the experimental static dielectric constant ($\varepsilon_0 = 11$).[74–76] Test calculations using an energy cutoff of 500 eV or a larger $3 \times 3 \times 2$ supercell (720 atoms) show that the effect of energy cutoff is marginal and that the supercell size has an effect which should be less than about 0.05 eV (see Table S2†).

Since the formation energy of a defect depends on the chemical potential of the elements involved in creating the defect, we have determined the chemical potential of Zn (μ_{Zn}) and the chemical potential of P (μ_P) according to the following four relations:

$$\mu_{Zn} < 0,$$

$$\mu_P < 0,$$

$$\mu_{Zn} + 2\mu_P < \Delta H_f\,(ZnP_2),$$

$$3\mu_{Zn} + 2\mu_P = \Delta H_f\,(Zn_3P_2),$$

where: (i) the first relation means μ_{Zn} (referenced to the energy of Zn in bulk zinc) should be less than 0 eV to avoid formation of bulk zinc phase; (ii) the second relation means μ_P (referenced to the energy of P in bulk phosphorus) should be less than 0 eV to avoid formation of bulk phosphorus phase; (iii) the third relation means μ_{Zn} and μ_P are bound such that the secondary phase ZnP_2 will not form; and (iv) the last relation ensures thermodynamic stability of (compositionally stoichiometric) Zn_3P_2. Using the calculated heats of formation (per unit formula): ΔH_f (ZnP_2) = −0.91 eV and ΔH_f (Zn_3P_2) = −1.31 eV, the allowed chemical-potential region of Zn_3P_2 is determined and plotted in Fig. S1.† Due to strong phase competition from ZnP_2, the stable region of Zn_3P_2 is quite small. Two different chemical-potential points of the stable region: A ($\mu_{Zn} = -0.203$ eV, $\mu_P = -0.354$ eV) and B ($\mu_{Zn} = 0.0$ eV, $\mu_P = -0.658$ eV), which represent Zn-poor (P-rich) and Zn-rich (P-poor) equilibrium growth conditions, respectively, were used in computing the defect formation energies.

The formation energy of the H-related point defects in Zn_3P_2 also depends on the chemical potential of H (μ_H). In the H-rich limit, $\mu_H = 0$ eV [referenced to half the energy $E(H_2)$ of an H_2 molecule at $T = 0$ K]. We have also considered the familiar situation of annealing in H_2 gas at temperature T and partial pressure p, where μ_H is determined through equilibrium with H_2 gas. In this case, μ_H is a well-established function of T and p:

$$\mu_H(T,p) = \frac{1}{2}E(H_2) + \mu_H^{H_2\ gas}(T,p),$$

The $\mu_H^{H_2\ gas}(T, p)$ for moderate T and p can be obtained by an analytical expression arising from the ideal-gas model [see *e.g.*, eqn (21) of ref. 63]. In the main text, we considered $T = 400$ °C and $p = 0.01$ atm, which gives $\mu_H = -0.45$ eV.

Some defects like the phosphorus interstitial (P_i) and hydrogen-related defects involve large atomic relaxations. Their ground-state structures deviate considerably from the undistorted initial trial configurations. For these defects, care has been exercised in order to correctly determine their ground-state configurations. This includes, but not limited to, using a fairly large number of initial trial configurations (for different charge states). In the future, one can use the recently developed ShakeNBreak global potential-energy surface search method to help identify the ground-state defect structure.[77,78]

Finally, in order to check whether our choice of $\alpha = 0.32$ for the HSE mixing parameter describes correctly the localized hole state of P*i*0, the fulfillment of the generalized Koopmans' theorem has been examined.[79–81] We find the non-Koopmans energy for P*i*0, defined as $E_{NK} = \varepsilon(N) - [E(N+1) - E(N)]$, to be small (0.12 eV). Here, $\varepsilon(N)$ is the single-particle energy level of the localized hole state of P_i^0, and $E(N+1) - E(N)$ is the total-energy difference between P_i^- (with atomic positions fixed to those of P_i^0) and P_i^0. The electrostatic finite-size correction was only applied to the total energy of P_i^-, and E_{NK} may still contain a small finite-size error. We conclude that the self-interaction error is relatively small in the HSE description of the localized hole state of P_i^0. We have also used the standard HSE06 functional ($\alpha = 0.25$) to calculate the (0/−) transition level of the P_i, starting from the HSE06-calculated lattice parameters. The HSE06 band gap is 1.15 eV, not as close to experiment as the HSE ($\alpha = 0.32$) band gap (1.41 eV). The HSE06 calculations also find a split-interstitial configuration of P_i^0, and yield a (0/−) transition level 0.54 eV above the VBM, compared to the value of 0.69 eV from the HSE calculation with $\alpha = 0.32$.

Conflicts of interest

There are no conflicts of interest to declare.

Acknowledgements

This work was supported by the U.S. Department of Energy, Office of Science, Basic Energy Sciences under award number DE-SC0023509. This research used resources of the National Energy Research Scientific Computing Center (NERSC), a DOE Office of Science User Facility supported by the Office of Science of the U.S. Department of Energy under contract no. DE-AC02-05CH11231 using NERSC award BES-ERCAP0023830.

References

1 C. Wadia, A. P. Alivisatos and D. M. Kammen, *Environ. Sci. Technol.*, 2009, **43**, 2072–2077.
2 Y. S. Lee, M. Bertoni, M. K. Chan, G. Ceder and T. Buonassisi, in *2009 34th IEEE Photovoltaic Specialists Conference (PVSC)*, DOI: DOI: 10.1109/PVSC.2009.5411314.
3 E. A. Fagen, *J. Appl. Phys.*, 1979, **50**, 6505–6515.
4 T. Suda, T. Nishimoto and S. Kurita, *J. Cryst. Growth*, 1988, **86**, 430–435.
5 N. C. Wyeth and A. Catalano, *J. Appl. Phys.*, 1979, **50**, 1403–1407.
6 G. M. Kimball, A. M. Müller, N. S. Lewis and H. A. Atwater, *Appl. Phys. Lett.*, 2009, **95**, 112103.

 This journal is © The Royal Society of Chemistry 2023

Published on 10 september 2023. Downloaded on 17.10.2024 19:53:00.

7 W. Shockley and H. J. Queisser, *J. Appl. Phys.*, 1961, **32**, 510–519.
8 M. Bhushan and A. Catalano, *Appl. Phys. Lett.*, 1981, **38**, 39–41.
9 P. S. Nayar and A. Catalano, *Appl. Phys. Lett.*, 1981, **39**, 105–107.
10 T. Suda, M. Kobayashi, A. Kuroyanagi and S. Kurita, *Jpn. J. Appl. Phys.*, 1982, **21**, 63.
11 M. Bhushan, *Appl. Phys. Lett.*, 1982, **40**, 51–53.
12 G. M. Kimball, N. S. Lewis and H. A. Atwater, in *35th IEEE Photovoltaic Specialists Conference (PVSC)*, DOI: DOI: 10.1109/PVSC.2010.5614641.
13 M. Zamani, E. Stutz, S. Escobar, R. R. Zamani, R. Paul, J.-B. Leran, M. Dimitrievska and A. Fontcuberta i Morral, *J. Phys.: Energy*, 2021, **3**, 034011.
14 R. Paul, N. Humblot, S. E. Steinvall, E. Z. Stutz, S. S. Joglekar, J.-B. Leran, M. Zamani, C. Cayron, R. Logé, A. G. del Aguila, Q. Xiong and A. F. I. Morral, *Cryst. Growth Des.*, 2020, **20**, 3816–3825.
15 J. P. Bosco, G. M. Kimball, N. S. Lewis and H. A. Atwater, *J. Cryst. Growth*, 2013, **363**, 205–210.
16 J. W. Andreasen, E. Arca, J. W. Bowers, M. Bär, J. Breternitz, P. J. Dale, M. Dimitrievska, D. J. Fermin, A. Ganose, C. J. Hages, T. Hobson, R. Jaramillo, S. R. Kavanagh, P. Kayastha, R. Kondrotas, J. Lee, J. D. Major, S. Mandati, D. B. Mitzi, D. O. Scanlon, S. Schorr, J. J. S. Scragg, B. Shin, S. Siebentritt, M. Smiles, M. Sood, K. V. Sopiha, N. Spalatu, M. Sutton, T. Unold, M. Valdes, A. Walsh, M. Wang, X. Wang, T. P. Weiss, Y. W. Woo, R. Woods-Robinson and D. Tiwari, *Faraday Discuss.*, 2022, **239**, 287–316.
17 R. Paul, S. W. Tabernig, J. Reñé Sapera, J. Hurni, A. Tiede, X. Liu, D. A. Damry, V. Conti, M. Zamani, S. Escobar Steinvall, M. Dimitrievska, E. Alarcon-Lladó, V. Piazza, J. Boland, F.-J. Haug, A. Polman and A. Fontcuberta i Morral, *Sol. Energy Mater. Sol. Cells*, 2023, **256**, 112349.
18 A. Catalano and R. B. Hall, *J. Phys. Chem. Solids*, 1980, **41**, 635–640.
19 S. Fuke, Y. Takatsuka, K. Kuwahara and T. Imai, *J. Cryst. Growth*, 1988, **87**, 567–570.
20 A. Kuroyanagi and T. Suda, *J. Cryst. Growth*, 1990, **100**, 1–4.
21 R. Katsube, H. Hayashi, A. Nagaoka, K. Yoshino, Y. Nose and Y. Shirai, *Jpn. J. Appl. Phys.*, 2016, **55**, 041201.
22 S. Demers and A. van de Walle, *Phys. Rev. B: Condens. Matter Mater. Phys.*, 2012, **85**, 195208.
23 W.-J. Yin and Y. Yan, *J. Appl. Phys.*, 2013, **113**, 013708.
24 E. Z. Stutz, S. P. Ramanandan, M. Flór, R. Paul, M. Zamani, S. Escobar Steinvall, D. A. Sandoval Salaiza, C. Xifra Montesinos, M. C. Spadaro, J.-B. Leran, A. P. Litvinchuk, J. Arbiol, A. Fontcuberta i Morral and M. Dimitrievska, *Faraday Discuss.*, 2022, **239**, 202–218.
25 R. Paul, V. Conti, M. Zamani, S. Escobar-Steinvall, H. Sánchez-Martín, C. Gastaldi, M. A. Ionescu, I. Íñiquez-de-la-Torre, M. Dimitrievska, A. Fontcuberta i Morral and V. Piazza, *Sol. Energy Mater. Sol. Cells*, 2023, **252**, 112194.
26 J. Misiewicz, *J. Phys. Chem. Solids*, 1989, **50**, 1013–1022.
27 T. Suda and R. H. Bube, *Appl. Phys. Lett.*, 1984, **45**, 775–777.
28 K. Sierański, J. Szatkowski and A. Hajdusianek, *Phys. Status Solidi A*, 2017, **214**, 1600553.
29 T. Suda, *J. Cryst. Growth*, 1990, **99**, 625–629.
30 T. L. Chu, S. S. Chu, K. Murthy, E. D. Stokes and P. E. Russell, *J. Appl. Phys.*, 1983, **54**, 2063–2068.
31 E. Papazoglou and T. W. F. Russell, *J. Vac. Sci. Technol., A*, 1987, **5**, 3378–3382.
32 J. Long, *J. Electrochem. Soc.*, 1983, **130**, 725.
33 K. Kakishita, K. Aihara and T. Suda, *Sol. Energy Mater. Sol. Cells*, 1994, **35**, 333–340.
34 A. M. Hermann, A. Madan, M. W. Wanlass, V. Badri, R. Ahrenkiel, S. Morrison and C. Gonzalez, *Sol. Energy Mater. Sol. Cells*, 2004, **82**, 241–252.
35 K. Kakishita, S. Ikeda and T. Suda, *J. Cryst. Growth*, 1991, **115**, 793–797.
36 K. Kakishita, S. Kondo and T. Suda, *Nucl. Instrum. Methods Phys. Res., Sect. B*, 1997, **121**, 175–178.
37 T. Suda, T. Miyakawa and S. Kurita, *J. Cryst. Growth*, 1988, **86**, 423–429.
38 M. Sharma, M. Mushrush, R. J. Wright, N. Shinkel, S. Sprague, S. Rozeveld, M. Woodward, K. Kearns, P. Small and C. Todd, *Thin Solid Films*, 2015, **591**, 32–38.
39 F. C. Wang, A. L. Fahrenbruch and R. H. Bube, *J. Appl. Phys.*, 1982, **53**, 8874–8879.
40 R. Bube, *Photoelectronic Properties of Zinc Phosphide Crystals, Films, and Heterojunctions. Quarterly Progress Report No. 11, October 1–December 31*, 1981, DOI: DOI: 10.2172/5664191.
41 M. S. Casey, A. L. Fahrenbruch and R. H. Bube, *J. Appl. Phys.*, 1987, **61**, 2941–2946.
42 C. G. Van de Walle, *Phys. Rev. Lett.*, 2000, **85**, 1012–1015.
43 S. Limpijumnong and C. G. Van de Walle, *Phys. Status Solidi B*, 2001, **228**, 303–307.
44 J. L. Lyons, A. Janotti and C. G. Van de Walle, *Phys. Rev. Lett.*, 2012, **108**, 156403.
45 K. Kakishita, K. Aihara and T. Suda, *Appl. Surf. Sci.*, 1994, **79–80**, 281–286.
46 H. J. von Bardeleben, J. L. Cantin, U. Gerstmann, A. Scholle, S. Greulich-Weber, E. Rauls, M. Landmann, W. G. Schmidt, A. Gentils, J. Botsoa and M. F. Barthe, *Phys. Rev. Lett.*, 2012, **109**, 206402.
47 S. B. Zhang, S.-H. Wei and A. Zunger, *J. Appl. Phys.*, 1998, **83**, 3192–3196.
48 A. Walsh and A. Zunger, *Nat. Mater.*, 2017, **16**, 964–967.
49 M. C. Spadaro, S. Escobar Steinvall, N. Y. Dzade, S. Martí-Sánchez, P. Torres-Vila, E. Z. Stutz, M. Zamani, R. Paul, J.-B. Leran, A. Fontcuberta i Morral and J. Arbiol, *Nanoscale*, 2021, **13**, 18441–18450.
50 K. Sieralfeki and J. Szatkowski, *Phys. Status Solidi A*, 1989, **111**, K57.
51 W. Shockley and W. T. Read, *Phys. Rev.*, 1952, **87**, 835–842.
52 R. N. Hall, *Phys. Rev.*, 1952, **87**, 387.
53 J. S. Park, S. Kim, Z. Xie and A. Walsh, *Nat. Rev. Mater.*, 2018, **3**, 194–210.
54 M. H. Du, *J. Mater. Chem. A*, 2014, **2**, 9091–9098.
55 A. Alkauskas, Q. Yan and C. G. Van de Walle, *Phys. Rev. B: Condens. Matter Mater. Phys.*, 2014, **90**, 075202.

Published on 10 september 2023. Downloaded on 17.10.2024 19:53:00.

56 L. Shi, K. Xu and L.-W. Wang, *Phys. Rev. B: Condens. Matter Mater. Phys.*, 2015, **91**, 205315.
57 J. Li, Z.-K. Yuan, S. Chen, X.-G. Gong and S.-H. Wei, *Chem. Mater.*, 2019, **31**, 826–833.
58 S. Kim, J.-S. Park, S. N. Hood and A. Walsh, *J. Mater. Chem. A*, 2019, **7**, 2686–2693.
59 X. Zhang, M. E. Turiansky, J.-X. Shen and C. G. Van de Walle, *J. Appl. Phys.*, 2022, **131**, 090901.
60 S. Lany and A. Zunger, *Phys. Rev. B: Condens. Matter Mater. Phys.*, 2008, **78**, 235104.
61 C. Freysoldt, B. Grabowski, T. Hickel, J. Neugebauer, G. Kresse, A. Janotti and C. G. Van de Walle, *Rev. Mod. Phys.*, 2014, **86**, 253–305.
62 D. Broberg, K. Bystrom, S. Srivastava, D. Dahliah, B. A. D. Williamson, L. Weston, D. O. Scanlon, G.-M. Rignanese, S. Dwaraknath, J. Varley, K. A. Persson, M. Asta and G. Hautier, *npj Comput. Mater.*, 2023, **9**, 72.
63 B. Aradi, A. Gali, P. Deák, J. E. Lowther, N. T. Son, E. Janzén and W. J. Choyke, *Phys. Rev. B: Condens. Matter Mater. Phys.*, 2001, **63**, 245202.
64 J. E. Northrup, R. Di Felice and J. Neugebauer, *Phys. Rev. B: Condens. Matter Mater. Phys.*, 1997, **56**, R4325–R4328.
65 C. G. Van de Walle and J. Neugebauer, *Nature*, 2003, **423**, 626–628.
66 C. G. V. d. Walle and J. Neugebauer, *Annu. Rev. Mater. Res.*, 2006, **36**, 179–198.
67 S. J. Pearton, J. W. Corbett and T. S. Shi, *Appl. Phys. A*, 1987, **43**, 153–195.
68 J. Chevallier and M. Aucouturier, *Annu. Rev. Mater. Sci.*, 1988, **18**, 219–256.
69 G. Kresse and J. Furthmüller, *Comput. Mater. Sci.*, 1996, **6**, 15–50.
70 G. Kresse and J. Furthmüller, *Phys. Rev. B: Condens. Matter Mater. Phys.*, 1996, **54**, 11169–11186.
71 J. Heyd, G. E. Scuseria and M. Ernzerhof, *J. Chem. Phys.*, 2003, **118**, 8207–8215.
72 R. Katsube and Y. Nose, *J. Cryst. Growth*, 2017, **459**, 95–99.
73 D. Broberg, B. Medasani, N. E. R. Zimmermann, G. Yu, A. Canning, M. Haranczyk, M. Asta and G. Hautier, *Comput. Phys. Commun.*, 2018, **226**, 165–179.
74 C. Freysoldt, J. Neugebauer and C. G. Van de Walle, *Phys. Rev. Lett.*, 2009, **102**, 016402.
75 Y. Kumagai and F. Oba, *Phys. Rev. B: Condens. Matter Mater. Phys.*, 2014, **89**, 195205.
76 O. Madelung, in *Semiconductors: Data Handbook*, Springer Berlin Heidelberg, 2004, pp. 173–244, DOI: DOI: 10.1007/978-3-642-18865-7_4.
77 I. Mosquera-Lois, S. R. Kavanagh, A. Walsh and D. O. Scanlon, *J. Open Source Softw.*, 2022, **7**, 4817.
78 I. Mosquera-Lois, S. R. Kavanagh, A. Walsh and D. O. Scanlon, *npj Comput. Mater.*, 2023, **9**, 25.
79 S. Lany and A. Zunger, *Phys. Rev. B: Condens. Matter Mater. Phys.*, 2009, **80**, 085202.
80 S. Lany and A. Zunger, *Phys. Rev. B: Condens. Matter Mater. Phys.*, 2010, **81**, 205209.
81 T. Gake, Y. Kumagai and F. Oba, *Phys. Rev. Mater.*, 2019, **3**, 044603.

 This journal is © The Royal Society of Chemistry 2023